10-13-2020

Dynamics of PDMS- g-PDMS Bottlebrush Polymers by Broadband Dielectric Spectroscopy

Bruno Jakobi
Louisiana State University

Karin J. Bichler
Louisiana State University

Anna Sokolova
Australian Nuclear Science and Technology Organisation

Gerald J. Schneider
Louisiana State University

Recommended Citation

Jakobi, B., Bichler, K., Sokolova, A., & Schneider, G. (2020). Dynamics of PDMS- g-PDMS Bottlebrush Polymers by Broadband Dielectric Spectroscopy. *Macromolecules, 53* (19), 8450-8458. https://doi.org/10.1021/acs.macromol.0c01277

Dynamics of PDMS-g-PDMS Bottlebrush Polymers by Broadband Dielectric Spectroscopy

Bruno Jakobi[1*], Karin J. Bichler[2], Anna Sokolova[3], Gerald J. Schneider[1,2*]

[1] Louisiana State University, Department of Chemistry, 70803 Baton Rouge, USA

[2] Louisiana State University, Department of Physics and Astronomy, 70803 Baton Rouge, USA

[3] Australia Center for Neutron Scattering, ANSTO, New Illawarra Road, Lucas Heights 2234, Australia

Email:

Bruno Jakobi: bjakob1@lsu.edu

Gerald J. Schneider: gjschneider@lsu.edu

Table of Content Figure

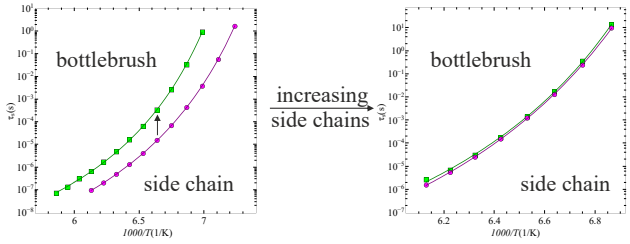

Keywords

Bottlebrush, Polymer, PDMS, Segmental Dynamics, Dielectric Spectroscopy, Neutron Scattering

Abstract

Poly(dimethylsiloxane) (PDMS) based bottlebrush polymers, PDMS-g-PDMS, have been synthesized by anionic polymerization in combination with a condensation based grafting reaction. Bottlebrush polymers show intriguing features, e.g., extremely low viscosities. Hereby studies of their dynamics are rare. Therefore, we focus on the segmental relaxation by broadband dielectric spectroscopy. An increasing cross-sectional radius proportional to the increasing side chain length has been observed by small-angle neutron scattering over three samples. A comparison of the segmental relaxation times of the bottlebrushes with the respective linear chains reveals slower dynamics in the former. For longer chains this effect vanishes.

Introduction

Bottlebrush polymers count to the branched polymers. Hereby, a high number of linear side chains are covalently bonded to a linear backbone, preventing the backbone from adopting a random coil conformation.[1] Changing the ratio of side chain to backbone length strongly influences the shape of bottlebrush polymers. This enables the synthesis of various structures ranging from elongated to spherical objects.[2-4] Several possible applications originate from the structural features, ranging from lubricants, to solvent free elastomers[5] up to surface modifications[6] or drug delivery agents[7].

Investigations based on the dynamics are rare. So far, the main focus of study is the difference in flow behavior compared to linear polymers, as determined by rheology.[8-9] Viscosity of polymers is related to their glass transition temperature, T_g, defined by $T_g = T(\eta_0 = 10^{12}$ Pa s).[10] A similar expression exists for the segmental relaxation time, τ_s, often measured by dielectric spectroscopy, i.e., $T_g = T(\tau_s = 100$ s).[11] However, studies based on the segmental relaxation behavior of

homopolymer bottlebrushes compared to their linear side chains are missing. The dielectric relaxation properties of heteropolymer bottlebrushes have been investigated in comparison to their respective backbone and side chain polymers.[12-14]

In this publication we are focusing on the segmental relaxation of poly(dimethylsiloxane) based bottlebrush, PDMS-g-PDMS, polymers compared to their respective linear PDMS side chains. For that, a synthesis route towards PDMS-g-PDMS bottlebrush polymers by the grafting-to method has been developed. This approach enables us to investigate the relaxation behavior of the single components prior to the grafting process. Furthermore, by using the same polymer for backbone and side chains, we minimize the risk of nano- or microphase separation. These phenomena are known to influence or constrain the dynamics of polymers with side chains, e.g., poly(alkylene oxide)s and poly(alkyl acrylate)s.[15-16]

Analysis

Small-Angle Neutron Scattering

For systems having a Kuhn length, ℓ_k, and contour length, L, much larger than the cross-sectional radius, R, the formfactor can be obtained by the decoupling approximation. Hereby, the backbone contour length (Figure 1 left), is treated separately from the side chains, i.e., the cross section (Figure 1 right).[17]

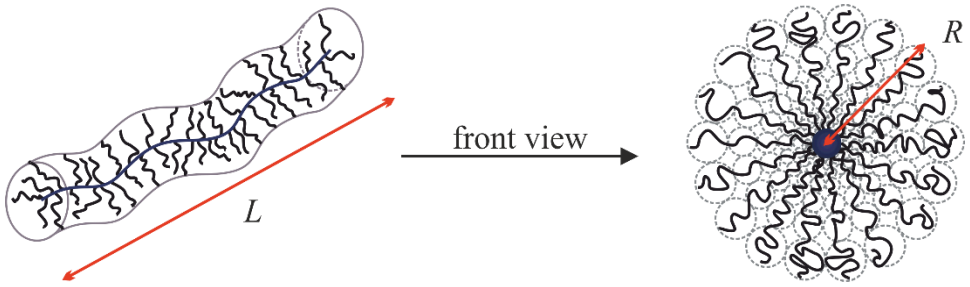

Figure 1. Pictorial representation of an elongated bottlebrush polymer, showing the side (left) and front view (right), with contour length, L, and cross-sectional radius, R.

The backbone is assumed to have an expanded conformation due to the high grafting density. However, because of the attached side chains, the overall structure is still flexible. Therefore, the backbone can be approximated by a semiflexible polymer chain, whereby the side chains are considered via the cross section by applying the Fourier transformation of the star like density profile, including the Flory exponent ν.[4, 18]

$$\varphi(r)_{star} = \frac{r^{\frac{1-3\nu}{\nu}}}{\left(1+\exp\left(\frac{r-R}{\sigma R}\right)\right)} \quad (1)$$

Here, the radial monomer density distribution[19] is multiplied by the Fermi cut-off function to ensure a smooth decay at the outermost radius R including the smearing parameter σ.

The total scattering function for elongated bottlebrush polymer can be written as[4]

$$I(Q) = \Phi V_{total} \Delta\rho^2 \cdot \left(P_{SPC}(Q) \cdot P_{CS}(Q) + a \cdot \frac{P_{blob}(Q)}{1 + \nu_{EV} P_{blob}(Q)} \right) \quad (2)$$

with volume concentration, Φ, the contrast, $\Delta\rho$, and the total volume, V_{total}, of the polymer, including all side chains and the backbone. It can be determined by using the molecular weight, M_w,

$$V_{total} = V_{side\ chain} \cdot f + V_{backbone} \quad (3)$$

with number of side chains, f, and volume, $V_i = \frac{M_{w_i}}{\varrho_i N_A}$, associated with side chains and backbone and the respective mass density, ϱ_i. The form factor $P_{SPC}(Q)$ stands for an infinitely thin, semiflexible polymer chain including excluded volume effects as described by Pedersen *et al.*[20], method 3, and Chen *et al.*[18] The final model for the semiflexible polymer chain has three adjustable parameters, the Kuhn length, ℓ_k, the Flory exponent, ν, and the cylinder contour length, L.

The form factor of the cross section, $P_{CS}(Q)$, can be calculated by a two-dimensional Fourier transformation of the star like density profile, equation (1). This reads as

$$P_{CS}(Q) = \left| \frac{\int_0^R \varphi(r)_{star} \cdot J_0(Qr) r\, dr}{\int_0^R \varphi(r)_{star} r dr} \right|^2 \quad (4)$$

with J_0 denoting the zeroth-order Bessel function of first kind and r the radial distance from the backbone. The dimension of our bottlebrush cross section is finite, therefore the outer radius, R, can be taken for the upper integration limit of the Fourier transformation instead of infinity. For the description of the internal structure within the cross section, a blob contribution, scaled with the prefactor a, is added to the form factor, considering the excluded volume, ν_{EV}. With ν_{EV} overlapping chains are considered and subtracted from the overall contribution. The form factor for the blob contribution, $P(Q)_{blob}$, can be described as:

$$P(Q)_{blob} = \exp\left(-\frac{Q^2\xi^2}{3}\right) + \left(\frac{d_f}{\xi^{d_f}}\right)\Gamma\left(\frac{d_f}{2}\right)\left(\frac{\mathrm{erf}\left(\frac{Qk\xi}{\sqrt{6}}\right)^3}{Q}\right)^{d_f} \quad (5)$$

Here, $k = 1.06$ is an empirical constant, ξ the radius of gyration and d_f the fractal dimension of the scattered particle which is typically $d_f = 2$ for melt or Θ-conditions or $d_f = 1.7$ for so called good solvent conditions. This parameter is connected to the Flory exponent, ν, with $d_f = 1/\nu$. The typical value for melt or Θ-condition is $\nu = 0.5$, whereby for good solvent $\nu = 0.588$, as predicted by perturbation theory.[21]

Broadband Dielectric Spectroscopy

The PDMS based bottlebrush polymers have only a dipole moment perpendicular to the polymer chain, in both, backbone and the side chains, and are thus type B polymers. Therefore, by using dielectric spectroscopy, only the segmental dynamics are probed.

The Debye model is the simplest description of a relaxation process. The complex dielectric function, $\epsilon^*(\omega)$, is defined as

$$\epsilon^*(\omega) = \epsilon_\infty + \frac{\Delta\epsilon}{1 + i\omega\tau_D} \quad (6)$$

with τ_D as the characteristic relaxation time of the system.[22] However, most of the time, the observed processes are non-ideal and the Debye model is not applicable. The empirical Havriliak-Negami function (HN), an adaption of the Debye model for non-ideal, i.e., asymmetric, relaxation processes, is used to describe the dielectric data in the frequency domain.[23]

$$\epsilon^*_{HN}(\omega) = \epsilon_\infty + \frac{\Delta\epsilon}{(1 + (i\omega\tau_{HN})^\beta)^\gamma} \quad (7)$$

Here, β and γ are shape parameters, describing the asymmetric broadening of the relaxation peak with the restrictions of $0 < \beta \leq 1$ and $0 < \gamma \cdot \beta \leq 1$. This complex function can also be split in a real and an imaginary part

$$\epsilon'_{HN}(\omega) = \epsilon_\infty + \Delta\epsilon\, r(\omega) \cos[\gamma\psi(\omega)]$$
$$\epsilon''_{HN}(\omega) = \Delta\epsilon\, r(\omega) \sin[\gamma\psi(\omega)] \tag{8}$$

with

$$r(\omega) = \left[1 + 2(\omega\tau_{HN})^\beta \cos\left(\frac{\beta\pi}{2}\right) + (\omega\tau_{HN})^{2\beta}\right]^{-\frac{\gamma}{2}}$$
$$\psi(\omega) = \arctan\left[\frac{\sin\left(\frac{\beta\pi}{2}\right)}{(\omega\tau_{HN})^{-\beta} + \cos\left(\frac{\beta\pi}{2}\right)}\right] \tag{9}$$

This results in the Havriliak-Negami relaxation time τ_{HN}.[22] However, τ_{HN} does not represent the "real" relaxation time τ_s, because it is slightly shifted due to the asymmetry of the relaxation peak. In order to correct this, the following equation needs to be applied.[24-27]

$$\frac{1}{\tau_s} = \frac{1}{\tau_{HN}}\left[\sin\left(\frac{\beta\pi}{2+2\gamma}\right)\right]^{\frac{1}{\beta}}\left[\sin\left(\frac{\beta\gamma\pi}{2+2\gamma}\right)\right]^{-\frac{1}{\beta}} \tag{10}$$

The temperature dependence of the segmental relaxation can be described with the Vogel-Fulcher-Tammann (VFT) equation.

$$\tau_s = \tau_\infty \exp\left(\frac{A}{T - T_0}\right) \tag{11}$$

Experimental Methods

Gel-Permeation Chromatography with Multi Angle Laser Light Scattering (GPC-MALLS)

For all Gel-Permeation Chromatography with Multi-Angle Laser Light Scattering (GPC-MALLS) measurements a GPC with two 500 mL HL syringe pumps from Teledyne Isco Inc., a Rheodyne manual injection valve from Kinesis Inc., three Phenogel 5 µm columns (300 × 7.8 mm) from Phenomenex, a Dawn Eos 18-angle static light scattering detector from Wyatt Technology Corporation, and a L-7490 differential Refractive Index (dRI) detector from Hitachi were used. The Astra software package was used for data collection and treatment.

Small-Angle Neutron Scattering (SANS)

Small-angle neutron scattering (SANS) experiments have been performed with the Bilby instruments at the Australian Centre for Neutron Scattering (ACNS) in Sydney, Australia.[28-29] The monochromatic mode has been used, with a wavelength of $\lambda = 6$ Å and a resolution of $\frac{\Delta\lambda}{\lambda} = 10\%$. Bilby has two detector carriages which can move independently within the vacuum vessel. The detector carriages consist of one single rear detector and a complex front detector assembled of four equally sized panels, called curtains. Hereby, distances from the sample to the rear detector, the horizontal and the vertical curtains of 13.5 m, 1.9 m, and 0.9 m were used, with a separation of the left and right curtain of 0.175 m and 0.350 m and those of the top and bottom curtain equals to 0.150 m and 0.030 m. This allows to capture the Q-range from 0.003 Å^{-1} to 0.56 Å^{-1} with the momentum transfer $Q = \frac{4\pi}{\lambda}\sin\left(\frac{\vartheta}{2}\right)$ and scattering angle ϑ, within one measurement, without changing the detector arrangement. The data reduction was performed using Bilby specific suitable routines in MANTID.[30] After correction for empty cell scattering, transmission, and detector response, the data sets were radially averaged and transformed onto an absolute scale. All samples

were additionally background corrected by subtracting the corresponding contributing volume fraction of the solvent.

Broadband Dielectric Spectroscopy

The dielectric spectroscopy measurements were performed with a Broadband Dielectric Alpha Analyzer from Novocontrol GmbH. The instrument operates in a frequency range of 10^{-2} Hz – 10^{6} Hz. The available temperature range of $T = -150$ °C to $T = +500$ °C is controlled by a Quatro Cryosystem with a manufacturer specified accuracy of 0.1 °C by using an evaporated nitrogen stream. For the measurements, a temperature range of $T = -140$ °C to $T = -90$ °C with an increment of $\Delta T = 2.5$ °C was enough to move the segmental dynamics through the available frequency range. A waiting time of three minutes was set prior to each spectrum measurement, ensuring a temperature stability equal or better than 0.1 °C. To avoid crystallization, the sample was rapidly cooled down to $T = -140$ °C and measurements at all temperatures were conducted in the order from low to high temperatures.

Results and Discussion

Synthesis

In the synthesis of PDMS based homopolymer bottlebrush the focus has mainly been on the grafting of living PDMS, with active lithium silanolate chain ends, onto a chlorosilane functionalized backbone, i.e., poly(methyl-2-chlorodimethylsilylethylsiloxane) or poly(methylchlorosiloxane) (PMClS).[31-32] These reactions suffer from side reactions, typically suppressed in the anionic ring opening polymerization of PDMS. In this paper we explored a mild grafting reaction based on the iterative growth of linear oligo(dimethlsiloxane)s in combination with the palladium catalyzed chlorination of PMHS as a viable alternative for the use of living PDMS (Scheme 1).[33-34]

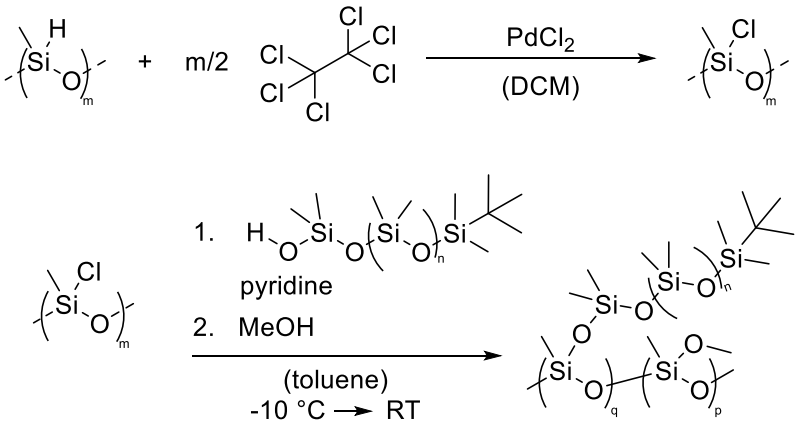

Scheme 1. Palladium catalyzed chlorination (top) and condensation based grafting reaction (bottom).

The precursor polymer, i.e., poly(methylhydrosiloxane) (PMHS), has been synthesized via the known cationic ring opening equilibration of tetramethylcyclotetrasiloxane and was split into fractions via precipitative fractionation with toluene as a solvent and acetonitrile as a non-solvent. For the activation of the backbone, a chlorination reaction of silanes catalyzed by palladium chloride with hexachloroethane as a chlorine source was adapted from Pongkittiphan *et al*.[33] The proposed mechanism involves the catalyst activation under production of hydrogen chloride.[33] To prevent

thermodynamic re-equilibration of the siloxane bonds, hydrogen chloride needs to be removed from the reaction. This was achieved by activating a $PdCl_2$/hexachloroethane mixture with chlorodimethylsilane followed by partial drying in vacuum. The reaction in pure dichloromethane resulted in a degree of chlorination of 99.7 % as determined by the disappearance of the SiH signal in the ^{1}H NMR spectrum. The chlorination was used for the *in situ* functionalization of PMHS directly before the grafting of side chains, avoiding the need for purification by filtration as needed in the chlorination with trichloroisocyanuric acid.[32]

Van Genabeek *et al.* reported the synthesis of monodisperse, low molecular weight PDMS by the repeated condensation of a oligo(dimethylsiloxane)s with silanol and chlorosilane chain ends, followed a reactivation of the chain ends for further condensation.[34] The condensation product, hydrochloric acid, is trapped by the addition of pyridine.[34] This concept is transferred towards the synthesis of bottlebrushes. The chlorosilane functionalized oligomer is replaced with PMClS as the electrophile and the silanol functionalized oligomer by a silanol terminated PDMS.

The applicability of the reaction is demonstrated via the synthesis of three bottlebrushes with long, middle, and short side chains, i.e., with 155, 25, and 4 repeating units, respectively (Table 1). Hereby, the long and middle side chains possess bulky tert-butyl end groups, whereas the short ones have slim SiH end groups. The grafting reaction results in similar grafting densities for the middle and long side chains and almost complete grafting for the shortest side chains. The molecular weight of the fraction of unreacted polymer remains unchanged after the grafting reaction, compared to the ungrafted side chains, as seen on the chromatograms of the bottlebrush with the longest side chains in Figure 2. The other chromatograms and ^{1}H NMR spectra can be found in Figure S1-S6 in the Supporting Information. The peak corresponding to the bottlebrush in the crude product mixture (black chromatograms) shows a low molecular weight tail. This part of the product mixture is removed after fractionation.

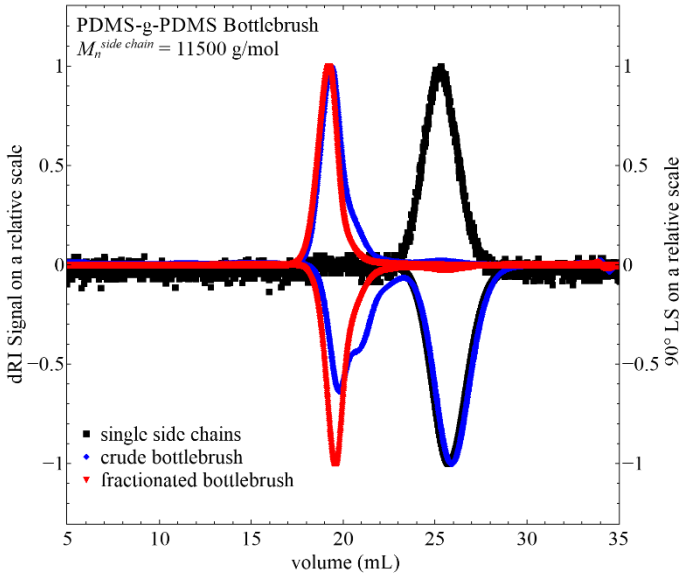

Figure 2. Differential Refractive Index (dRI) (down peak) and 90 ° Light Scattering (LS) (up peak) signal of the GPC-MALLS chromatogram on a relative scale for the single side chain (black), crude bottlebrush (blue), and fractionated bottlebrush (red) for the longest side chains.

Table 1. Number average molecular weight, M_n, PDI, and the grafting density, ρ^*, of the three bottlebrush samples and their constituents.

Name	single chain M_n (g/mol) (PDI)	bottlebrush M_n (kg/mol) (PDI) [ρ^*]
Short	298 (1.0)	95 (1.3) [89]
Middle	1800 (1.2)	157 (1.1) [30]
Long	11500 (1.1)	1106 (1.2) [41]
Backbone-short	16500 (1.1)	---
Backbone-middle/long	13500 (1.2)	---

Small-Angle Neutron Scattering

A low concentration, $\Phi = 0.5\%$, of the bottlebrush polymers in deuterated cyclohexane is measured to identify the pure form factor, $P(Q)$. For the sample, having the shortest side chains, $M_n^{side\ chain} = 298$ g/mol (blue circles), two kinks appear, as seen in Figure 3 (blue circles). While the first one is located at $Q \sim 0.01$ Å^{-1}, the second one is at $Q \sim 0.2$ Å^{-1}. In the region between these two kinks an intensity dependence of $I \propto Q^{-1.7}$ is found. This power law of 1.7 suggests the presence of elongated shapes with a semi-flexible structure in good solvent conditions.[4] Hereby, the first kink corresponds to the length, whereas the second one is attributed to the cross-sectional radius. With increasing side chain length, the second kink from $Q \sim 0.2$ Å^{-1} moves to smaller Q (Figure 3, green squares), while the kink at lower Q stays the same. This effect is caused by an increase of the cross-sectional radius through the longer side chains, while the overall length of the polymer stays the same. Both together show the independent modification of length and cross-sectional radius. Increasing the side chain length further to $M_n^{side\ chain} = 11500$ g/mol shifts both kinks even closer together resulting in a direct transition from low to intermediate Q-values, which suggest the appearance of an almost spherical shape (Figure 3, red diamonds).

All samples can be well described by the form factor, $P(Q)$, for elongated bottlebrush polymers, equation (2). The resulting fit parameters are summarized in Table 2.

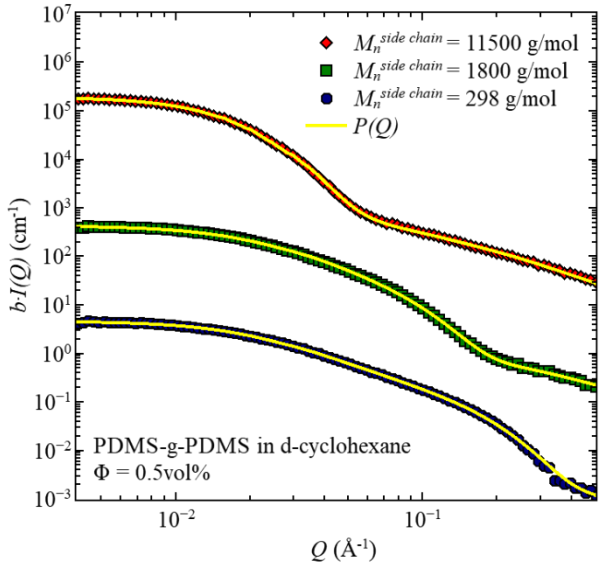

Figure 3. Scattering intensity, $I(Q)$, vs. momentum transfer, Q, of the three different PDMS-g-PDMS bottlebrush polymers in d-cyclohexane. Solid lines represent the description with the form factor $P(Q)$. For clarity, the data are shifted by a factor b in y-direction. Blue circles $b = 1$, green squares $b = 50$, and red diamonds $b = 5000$. Error bars are within symbol size and omitted.

Table 2. Contour length, L, radius, R, Kuhn length, ℓ_k, and blob size, ξ, of the three bottlebrush polymers. All errors are smaller than 1%. An additional table with the remaining fit parameters can be found in the Supporting Information.

Name	Short	Middle	Long
Length L (Å)	797.0	796.7	840.7
Radius R (Å)	4.8	8.7	47.2
Kuhn length ℓ_k (Å)	43.6	43.6	42.8
Blob size ξ (Å)	2.7	7.5	18.9

The fit parameters illustrate the independence of the Kuhn length, ℓ_k, from the side chain length while the contour length, L, increases. This is a consequence of the attachment of the side chains, as those located at the extremities of backbone cause its extension. This effect exists for all three samples but is most evident for the bottlebrush with the longest side chain. Only the radius and the

blob size are substantially influenced by the side chain variation. The Kuhn length of PDMS-g-PDMS seems to be significantly larger than the one of linear PDMS, $\ell_k^{PDSM} = 13$ Å.[35] This observation appears to be a common feature shared by a variety of bottlebrush polymers if compared to their respective linear counterparts.[4]

Broadband Dielectric Spectroscopy

All samples, together with the single side chains, i.e., PDMS-g-PDMS bottlebrush and linear PDMS, have been measured with dielectric spectroscopy. Since PDMS is a so-called type B polymer, dielectric spectroscopy has access to the segmental relaxation for the bottlebrush polymers and the single side chains, resulting in information about the segmental relaxation times, τ_s. However, the majority of the dipole moments are located in the side chains; therefore, the segmental relaxation of the bottlebrush polymers is dominated by the side chains.

This publication sets the focus on the pure segmental relaxation. However, the bottlebrush polymers also show the influence of the cold crystallization on the segmental relaxation, i.e., the α_c-relaxation, as known for linear PDMS.[36] This effect intensifies with increasing molecular weight of the side chains. In our samples, the α_c-relaxation is well pronounced only for the sample with the longest side chains, $M_n^{side\ chain} = 11500$ g/mol (Supporting Information Figure S8). For the other two samples, the crystallization is marginal due to the low molecular weight and does not allow to be extract a relaxation time. Since we are focusing on the pure segmental relaxation, the α_c-relaxation will not be discussed further.

The typical relaxation spectra obtained by dielectric spectroscopy for the PDMS-g-PDMS bottlebrush polymers (top row) and the respective linear PDMS side chains (bottom row) are shown in Figure 4.

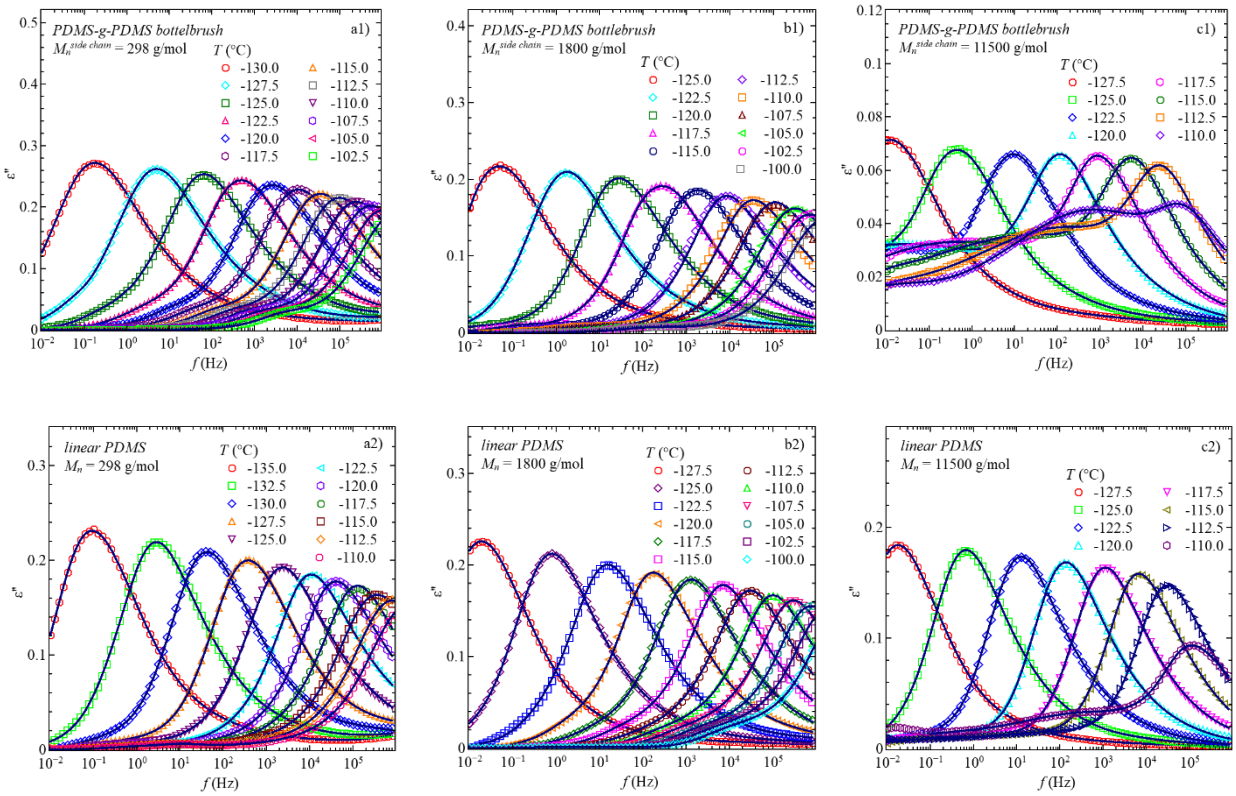

Figure 4. Imaginary part of the permittivity, ϵ'', vs. frequency, f, for the PDMS-g-PDMS bottlebrush polymers (top) compared with the respective linear PDMS side chains (bottom). Top row: a1: $M_n^{side\ chain} = 298$ g/mol, b1: $M_n^{side\ chain} = 1800$ g/mol, c1: $M_n^{side\ chain} = 11500$ g/mol. Bottom row: a2: $M_n = 298$ g/mol, b2: $M_n = 1800$ g/mol, c2: $M_n = 11500$ g/mol. Solid lines represent the best descriptions with Havriliak-Negami functions.

Here, in bottlebrush polymers as well as in the single side chains, a well pronounced relaxation peak is visible which shifts to higher frequencies with increasing temperature. This is associated with a decrease in relaxation time, τ_s, which is the reciprocal value of the frequency at the peak maximum. The data can be well described with a combination of Havriliak-Negami functions.

Normalizing the dielectric permittivity as well as the frequency to one allows to analyze the influence of the temperature on the shape of the relaxation peak (Figure 5). This comparison shows no effect of temperature on the segmental relaxation other than a changing relaxation time. This applies to all samples, regardless of the architecture of the polymer.

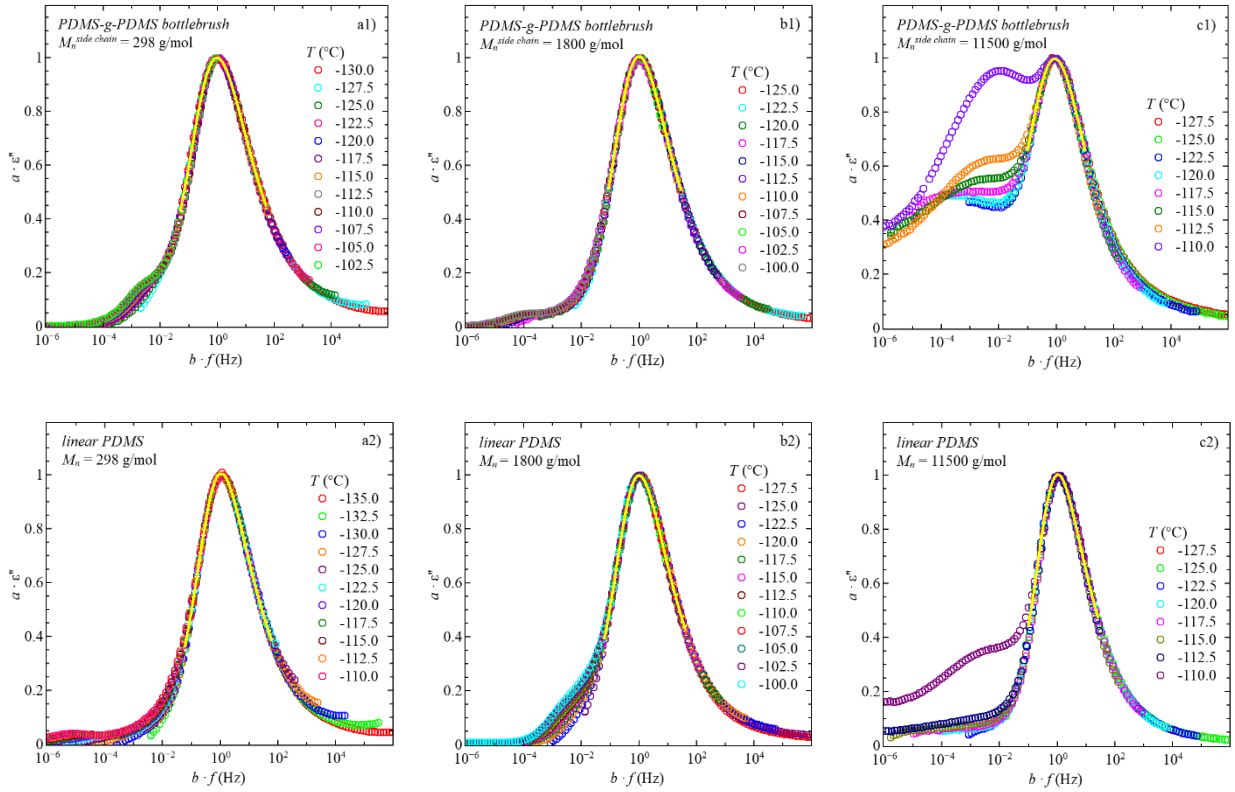

Figure 5. Normalized imaginary part of the permittivity, $a \cdot \epsilon''$, vs. normalized frequency, $b \cdot f$, for the PDMS-g-PDMS bottlebrush polymers (top) compared with the respective linear PDMS side chains (bottom). Top row: a1: $M_n^{side\ chain} = 298$ g/mol, b1: $M_n^{side\ chain} = 1800$ g/mol, c1: $M_n^{side\ chain} = 11500$ g/mol. Bottom row: a2: $M_n = 298$ g/mol, b2: $M_n = 1800$ g/mol, c2: $M_n = 11500$ g/mol. Solid lines represent the best descriptions with the Havriliak-Negami function.

Differences arising from the onset of the crystallization are visible at the low frequency sides. In case of the short and middle side chain length, this little onset is not developed enough to perform an adequate analysis for the α_c-relaxation. In contrast, for the bottlebrush polymer and the single side chains with $M_n^{side\ chain} = 11500$ g/mol (Figure 5 c1 and c2) pronounced deviations, caused by the α_c-relaxation, are visible at the left side.

The temperature independent shape of the α-relaxation peak simplifies the description of the data sets and allows to describe all temperatures by the HN model function. The parameters β and γ are hereby shared over all temperatures.[11, 37] The associated fit values of the relaxation peak can

be found in the Supporting Information. Therefore, the relaxation time associated with each single temperature can be calculated from the shift factors used for the normalization. This leads to the Havriliak-Negami relaxation time, τ_{HN}, which is transformed to the relaxation time, τ_s, connected to the position of the relaxation peak, by using equation (10).

Figure 6 illustrates the relaxation time dependence on the reciprocal temperature, which is a more convenient way to compare the relaxation behavior of the different materials. Hereby the temperature dependence follows the empirical VFT-law (equation (11)). The resulting fit parameters can be found in Table 3.

All samples have in common that the relaxation time decreases continuously with increasing temperature. However, comparing the bottlebrush polymer with the respective side chains shows an increased relaxation time. This effect depends on the molecular weight of the side chains and disappears for sufficiently high $M_n^{side\ chain}$. For the shortest side chain length (Figure 6a) the relaxation times are slowed down by $\sim$2.5 orders of magnitude and those for the middle side chains by $\sim$1.5 orders of magnitude (Figure 6b). Upon increasing the side chain length further, to $M_n^{side\ chain} = 11500$ g/mol, both samples, bottlebrush and single side chain, coincide over the entire temperature range and no increase of the relaxation time is observable (Figure 6c).

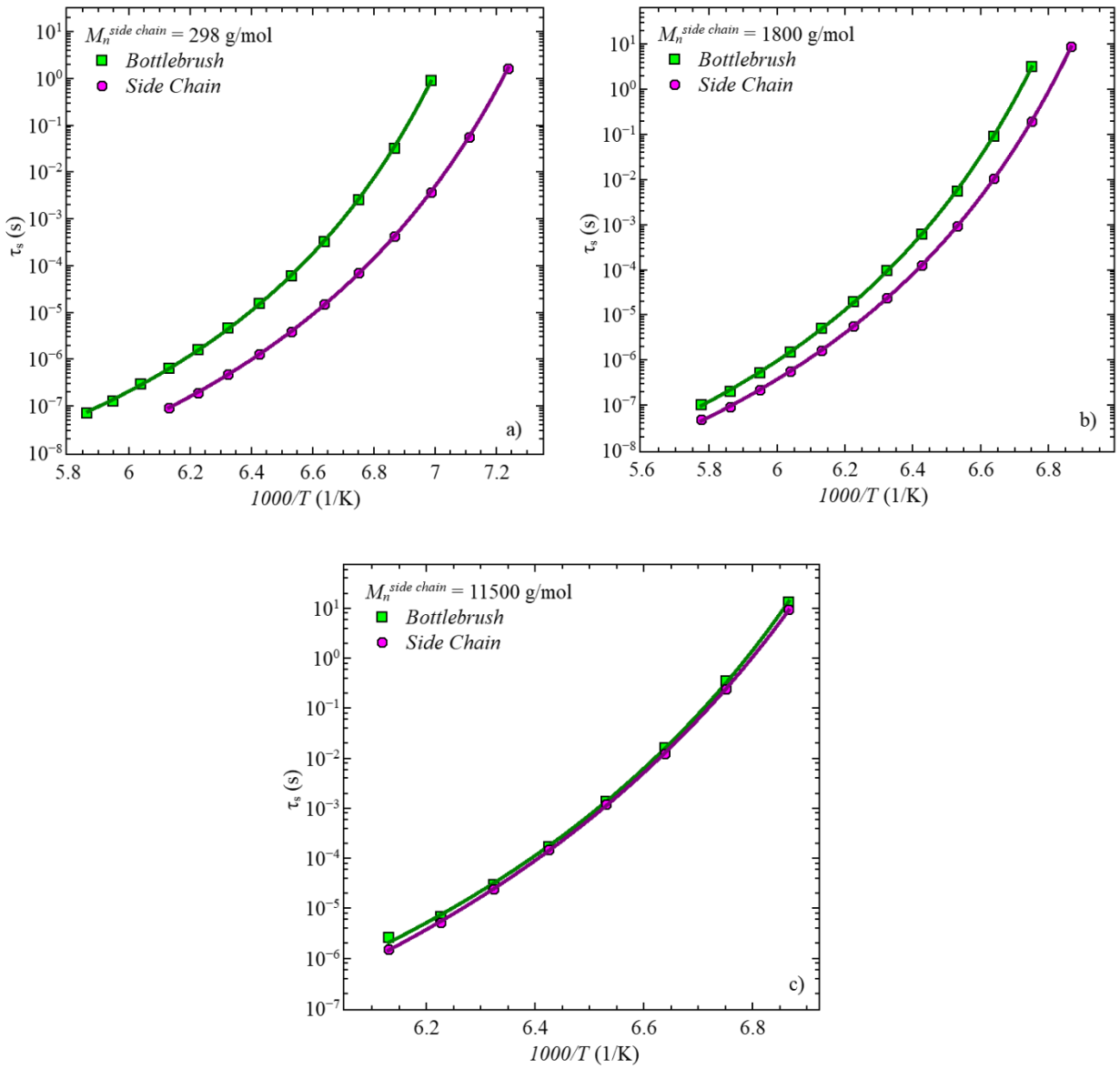

Figure 6. Segmental relaxation time, τ_s, vs. $1000/T$ for the PDMS-g-PDMS bottlebrush polymer compared with their respective single linear PDMS side chains. a) $M_n^{side\ chain} = 298$ g/mol, b) $M_n^{side\ chain} = 1800$ g/mol, c) $M_n^{side\ chain} = 11500$ g/mol. Solid lines are the best description with the VFT equation.

Table 3. Fit parameter for describing the temperature dependence of the segmental relaxation times from PDMS-g-PDMS bottlebrush polymer and their respective single side chain.

	Sample	τ_∞ (s)	A (K)	T_0 (K)
Bottlebrush	Short	$(12.3 \pm 2.3) \cdot 10^{-13}$	508 ± 11	124.5 ± 0.3
	Middle	$(13.4 \pm 3.9) \cdot 10^{-14}$	602 ± 17	128.6 ± 0.4
	Long	$(4.6 \pm 2.3) \cdot 10^{-14}$	654 ± 23	126.0 ± 0.4
Side Chain	Short	$(23.1 \pm 1.8) \cdot 10^{-14}$	572 ± 4	118.8 ± 0.1
	Middle	$(92.3 \pm 6.1) \cdot 10^{-15}$	608 ± 4	126.7 ± 0.1
	Long	$(5.6 \pm 1.3) \cdot 10^{-15}$	759 ± 12	123.9 ± 0.2

For each graph, the relaxation time of chains covalently bonded to a backbone is compared to those of linear chains with identical molecular weight. Strongest differences are observed in case of the lowest molar mass, equivalent to only four repeating units. Increasing the number of repeating units leads to a reduction of the differences in relaxation times, resulting in nearly overlapping VFT-graphs for the longest side chains. This is a strong indication that those segments in close proximity to the junction are affected the strongest, while there is less influence farther away from the backbone. This suggests a critical length above which segments have the same relaxation time as free chains. It may also suggest a gradual change from the inner to the outermost segments, that may even be considered as a gradient of relaxation times from strongly confined, at the junction, to free relaxation, equivalent to a linear chain.

Segmental relaxation is always connected to the glass transition temperature, which can be defined as the temperature, at which the condition for the relaxation time $\tau_s = 100$ s, i.e., $T_g = T(\tau_s = 100 \text{ s})$ is fulfilled.[22] Extracted values for the single side chains, as well as for the respective bottlebrush polymers are summarized in Table 4. Here differences are visible, depending on the

architecture and the molecular weight. In general, the glass transition temperature of the bottlebrush polymers is above the respective single side chains but in the same region. This trend matches the differences in segmental relaxation times. Similar results were also found for different hetero- and homopolymer bottlebrushes.[13, 38-39]

Table 4. Extracted glass transition temperature, T_g, from dielectric spectroscopy measurement for the single linear PDMS side chains and the respective bottlebrush polymers.

	Sample	$T_g\ (°C)$	$T_g\ (K)$
Bottlebrush	Short	-132.8 ± 0.2	140.4 ± 0.2
	Middle	-127.0 ± 0.5	146.2 ± 0.5
	Long	-128.6 ± 0.7	144.6 ± 0.7
Side Chains	Short	-137.3 ± 0.1	135.8 ± 0.1
	Middle	-128.8 ± 0.1	144.3 ± 0.1
	Long	-128.9 ± 0.2	144.3 ± 0.2

Therefore, the grafting process also increases the glass transition temperature, as expected by the slowed down segmental relaxation time. However, the temperature dependence of the relaxation times is still the same, independent of the architecture, which is in contrast to heteropolymer bottlebrush polymers.[13]

Conclusion

We have investigated the segmental relaxation behavior of PDMS-g-PDMS bottlebrush polymers depending on the side chain lengths. Therefore, three bottlebrushes with different side chain molecular weights have been synthesized, whereby in all cases the backbone length was kept

constant. This results in increasing cross-sectional radii, investigated by small-angle neutron scattering. The connected dynamical changes, inherent with the different side chain lengths, have been examined by broadband dielectric spectroscopy, measuring the segmental relaxation times, τ_s. By comparing the segmental relaxation behavior of the bottlebrush polymers with the respective single side chains, an increase in the segmental relaxation times is visible. Hereby, the strongest effect is apparent in the sample with the shortest side chains. By increasing the side chain length, the effect of an increased τ_s decreases. Finally, for the sample with the longest side chains, the segmental relaxation times coincide over the whole temperature range. This effect of the increased relaxation times originates from the grafting process and is independent of the grafting density. Consequently, the glass transition temperatures of bottlebrush polymers can be approximated with equal or higher values compared to those for the linear polymers equivalent to the side chains.

Acknowledgements

We acknowledge funding by the U.S. Department of Energy (DoE) under grant DE-SC0019050. We are also grateful for the access to the neutron scattering instruments, provided by Australian Nuclear Science and Technology Organisation (ANSTO).

Supporting Information

The supporting information is available free of charge at http://pubs.acs.org, including the experimental procedures, additional GPC-chromatograms, ^{1}H NMR, additional SANS fit parameter, fit values of the dielectric spectra, and temperature dependence of the relaxation times of α- and α_c-relaxation for the long chain sample.

References

1. Polymeropoulos, G.; Zapsas, G.; Ntetsikas, K.; Bilalis, P.; Gnanou, Y.; Hadjichristidis, N., 50th Anniversary Perspective: Polymers with Complex Architectures. *Macromolecules* **2017,** *50* (4), 1253-1290.

2. Pesek, S. L.; Xiang, Q.; Hammouda, B.; Verduzco, R., Small-Angle Neutron Scattering Analysis of Bottlebrush Backbone and Side Chain Flexibility. *Journal of Polymer Science Part B: Polymer Physics* **2017,** *55* (1), 104-111.

3. Pesek, S. L.; Li, X.; Hammouda, B.; Hong, K.; Verduzco, R., Small-Angle Neutron Scattering Analysis of Bottlebrush Polymers Prepared via Grafting-Through Polymerization. *Macromolecules* **2013,** *46* (17), 6998-7005.

4. Rathgeber, S.; Pakula, T.; Wilk, A.; Matyjaszewski, K.; Beers, K. L., On the Shape of Bottle-Brush Macromolecules: Systematic Variation of Architectural Parameters. *J Chem Phys* **2005,** *122* (12), 124904.

5. Daniel, W. F.; Burdynska, J.; Vatankhah-Varnoosfaderani, M.; Matyjaszewski, K.; Paturej, J.; Rubinstein, M.; Dobrynin, A. V.; Sheiko, S. S., Solvent-Free, Supersoft and Superelastic Bottlebrush Melts and Networks. *Nat Mater* **2016,** *15* (2), 183-9.

6. Pesek, S. L.; Lin, Y.-H.; Mah, H. Z.; Kasper, W.; Chen, B.; Rohde, B. J.; Robertson, M. L.; Stein, G. E.; Verduzco, R., Synthesis of Bottlebrush Copolymers based on Poly(dimethylsiloxane) for Surface Active Additives. *Polymer* **2016,** *98*, 495-504.

7. Müllner, M., Molecular Polymer Brushes in Nanomedicine. *Macromolecular Chemistry and Physics* **2016,** *217* (20), 2209-2222.

8. Dalsin, S. J.; Hillmyer, M. A.; Bates, F. S., Linear Rheology of Polyolefin-Based Bottlebrush Polymers. *Macromolecules* **2015,** *48* (13), 4680-4691.

9. Dalsin, S. J.; Hillmyer, M. A.; Bates, F. S., Molecular Weight Dependence of Zero-Shear Viscosity in Atactic Polypropylene Bottlebrush Polymers. *ACS Macro Letters* **2014,** *3* (5), 423-427.

10. Mauro, J. C.; Yue, Y.; Ellison, A. J.; Gupta, P. K.; Allan, D. C., Viscosity of Glass-Forming Liquids. *Proceedings of the National Academy of Sciences* **2009,** *106* (47), 19780.

11. Hintermeyer, J.; Herrmann, A.; Kahlau, R.; Goiceanu, C.; Rössler, E. A., Molecular Weight Dependence of Glassy Dynamics in Linear Polymers Revisited. *Macromolecules* **2008,** *41* (23), 9335-9344.

12. Staropoli, M.; Raba, A.; Hövelmann, C. H.; Appavou, M.-S.; Allgaier, J.; Krutyeva, M.; Pyckhout-Hintzen, W.; Wischnewski, A.; Richter, D., Melt Dynamics of Supramolecular Comb Polymers: Viscoelastic and Dielectric response. *Journal of rheology* **2017,** *61* (6), 1185-1196.

13. Grigoriadis, C.; Nese, A.; Matyjaszewski, K.; Pakula, T.; Butt, H.-J.; Floudas, G., Dynamic Homogeneity by Architectural Design – Bottlebrush Polymers. *Macromolecular Chemistry and Physics* **2012,** *213* (13), 1311-1320.

14. Nikovia, C.; Theodoridis, L.; Alexandris, S.; Bilalis, P.; Hadjichristidis, N.; Floudas, G.; Pitsikalis, M., Macromolecular Brushes by Combination of Ring-Opening and Ring-Opening Metathesis Polymerization. Synthesis, Self-Assembly, Thermodynamics, and Dynamics. *Macromolecules* **2018,** *51* (21), 8940-8955.

15. Beiner, M.; Huth, H., Nanophase Separation and Hindered Glass Transition in Side-Chain Polymers. *Nature Materials* **2003,** *2* (9), 595-599.

16. Gerstl, C.; Schneider, G. J.; Fuxman, A.; Zamponi, M.; Frick, B.; Seydel, T.; Koza, M.; Genix, A. C.; Allgaier, J.; Richter, D.; Colmenero, J.; Arbe, A., Quasielastic Neutron Scattering Study on the Dynamics of Poly(alkylene oxide)s. *Macromolecules* **2012,** *45* (10), 4394-4405.

17. Pedersen, J. S.; Schurtenberger, P., Cross-Section Structure of Cylindrical and Polymer-Like Micelles from Small-Angle Scattering Data. I. Test of Analysis Methods. *Journal of Applied Crystallography* **1996,** *29* (6), 646-661.

18. Chen, W.-R.; Butler, P. D.; Magid, L. J., Incorporating Intermicellar Interactions in the Fitting of SANS Data from Cationic Wormlike Micelles. *Langmuir* **2006,** *22* (15), 6539-6548.

19. Daoud, M.; Cotton, J. P., Star Shaped Polymers : A Model for the Conformation and its Concentration Dependence. *J. Phys. France* **1982,** *43* (3), 531-538.

20. Pedersen, J. S.; Schurtenberger, P., Scattering Functions of Semiflexible Polymers with and without Excluded Volume Effects. *Macromolecules* **1996,** *29* (23), 7602-7612.

21. Dozier, W. D.; Huang, J. S.; Fetters, L. J., Colloidal Nature of Star Polymer Dilute and Semidilute Solutions. *Macromolecules* **1991,** *24* (10), 2810-2814.

22. Kremer, F.; Schönhals, A., *Broadband Dielectric Spectroscopy*. Springer Berlin Heidelberg: 2012.

23. Strobl, G. R., *The Physics of Polymers: Concepts for Understanding Their Structures and Behavior*. Springer Berlin Heidelberg: 2013.

24. Díaz-Calleja, R., Comment on the Maximum in the Loss Permittivity for the Havriliak−Negami Equation. *Macromolecules* **2000,** *33* (24), 8924-8924.

25. Boersma, A.; Turnhout, J.; Wübbenhorst, M., Dielectric Characterization of a Thermotropic Liquid Crystalline Copolyesteramide: 1. Relaxation Peak Assignment. *Macromolecules* **1998,** *31*, 7453-7460.

26. Gerstl, C.; Schneider, G. J.; Pyckhout-Hintzen, W.; Allgaier, J.; Richter, D.; Alegría, A.; Colmenero, J., Segmental and Normal Mode Relaxation of Poly(alkylene oxide)s Studied by Dielectric Spectroscopy and Rheology. *Macromolecules* **2010,** *43* (11), 4968-4977.

27. Xing, K.; Chatterjee, S.; Saito, T.; Gainaru, C.; Sokolov, A. P., Impact of Hydrogen Bonding on Dynamics of Hydroxyl-Terminated Polydimethylsiloxane. *Macromolecules* **2016,** *49* (8), 3138-3147.

28. Sokolova, A.; Christoforidis, J.; Eltobaji, A.; Barnes, J.; Darmann, F.; Whitten, A. E.; de Campo, L., BILBY: Time-of-Flight Small Angle Scattering Instrument. *Neutron News* **2016,** *27* (2), 9-13.

29. Sokolova, A.; Whitten, A. E.; de Campo, L.; Christoforidis, J.; Eltobaji, A.; Barnes, J.; Darmann, F.; Berry, A., Performance and Characteristics of the BILBY Time-of-Flight Small-Angle Neutron Scattering Instrument. *Journal of Applied Crystallography* **2019,** *52* (1), 1-12.

30. Arnold, O.; Bilheux, J. C.; Borreguero, J. M.; Buts, A.; Campbell, S. I.; Chapon, L.; Doucet, M.; Draper, N.; Ferraz Leal, R.; Gigg, M. A.; Lynch, V. E.; Markvardsen, A.; Mikkelson, D. J.; Mikkelson, R. L.; Miller, R.; Palmen, K.; Parker, P.; Passos, G.; Perring, T. G.; Peterson, P. F.; Ren, S.; Reuter, M. A.; Savici, A. T.; Taylor, J. W.; Taylor, R. J.; Tolchenov, R.; Zhou, W.; Zikovsky, J., Mantid—Data Analysis and Visualization Package for Neutron Scattering and μ SR Experiments. *Nuclear Instruments and Methods in Physics Research Section A: Accelerators, Spectrometers, Detectors and Associated Equipment* **2014,** *764*, 156-166.

31. Chojnowski, J.; Cypryk, M.; Fortuniak, W.; Ścibiorek, M.; Rózga-Wijas, K., Synthesis of Branched Polysiloxanes with Controlled Branching and Functionalization by Anionic Ring-Opening Polymerization. *Macromolecules* **2003,** *36* (11), 3890-3897.

32. Bichler, K. J.; Jakobi, B.; Huber, S. O.; Gilbert, E. P.; Schneider, G. J., Structural Analysis of Ultrasoft PDMS-g-PDMS Shell-Only Particles. *Macromolecules* **2020,** *53* (1), 78-89.

33. Pongkittiphan, V.; Theodorakis, E. A.; Chavasiri, W., Hexachloroethane: a Highly Efficient Reagent for the Synthesis of Chlorosilanes from Hydrosilanes. *Tetrahedron letters* **2009,** *50* (36), 5080-5082.

34. van Genabeek, B.; de Waal, B. F. M.; Gosens, M. M. J.; Pitet, L. M.; Palmans, A. R. A.; Meijer, E. W., Synthesis and Self-Assembly of Discrete Dimethylsiloxane–Lactic Acid Diblock Co-oligomers: The Dononacontamer and Its Shorter Homologues. *Journal of the American Chemical Society* **2016,** *138* (12), 4210-4218.

35. Rubinstein, M.; Colby, R. H., *Polymer Physics*. OUP Oxford: 2003.

36. Lund, R.; Alegria, A.; Goitandia, L.; Colmenero, J.; González, M. A.; Lindner, P., Dynamical and Structural Aspects of the Cold Crystallization of Poly (Dimethylsiloxane)(PDMS). *Macromolecules* **2008,** *41* (4), 1364-1376.

37. Lunkenheimer, P.; Loidl, A., Dielectric Spectroscopy of Glass-Forming Materials: α-Relaxation and Excess Wing. *Chemical Physics* **2002,** *284* (1), 205-219.

38. Tsukahara, Y.; Namba, S.-i.; Iwasa, J.; Nakano, Y.; Kaeriyama, K.; Takahashi, M., Bulk Properties of Poly(macromonomer)s of Increased Backbone and Branch Lengths. *Macromolecules* **2001,** *34* (8), 2624-2629.

39. Hu, M.; Xia, Y.; McKenna, G. B.; Kornfield, J. A.; Grubbs, R. H., Linear Rheological Response of a Series of Densely Branched Brush Polymers. *Macromolecules* **2011,** *44* (17), 6935-6943.